Study of damages caused by proton irradiation on MCT n/p focal plane cooled arrays

Ségolène Dinand, Eric Deborniol, Nicolas Baier, Florent Rochette, Serena Rizzolo, Vincent Goiffon, Olivier Gravrand

Study of damages caused by proton irradiation on MCT n/p focal plane cooled arrays

Ségolène Dinand [a b c], Eric Deborniol [a], Nicolas Baier [a], Florent Rochette [a],
Serena Rizzolo [c], Vincent Goiffon [b],
Olivier Gravrand [a*]
[a] UGA-CEA-LETI, 17 av des Martyrs, 38054 Grenoble, France
[b] ISAE-SUPAERO, Université de Toulouse, 10 Av. Edouard Belin, 31400 Toulouse, France
[c] Airbus Defense and Space 31 Rue des Cosmonautes, 31400 Toulouse, France

ABSTRACT

HgCdTe (MCT) is a material system intensively used for IR sensing from space as it offers high detection performances. It is also considered as a relatively radhard material system as the performance degradation due to radiative space environment are usually not dramatic compared to other material systems. However, there is no clear understanding of the effect of displacement damage dose (DDD) or even total ionizing dose (TID) in this material system. In this communication, we present an extensive study of the damage due to protons on n/p MCT diodes sensing in the MW range. Both FPA full arrays, single diodes and MIS test structures have been irradiated with 63 MeV protons up to relatively high doses (8e11 protons/cm²). We will report about the evolution of dark current and noise degradation (mainly due to RTS), during and after irradiation, as well as after a thermal cycling up to 300K and even after a recovery annealing at higher temperature.

Keywords: MCT, MWIR, proton irradiation, gamma irradiation, dark current, RTS

1. INTRODUCTION

HgCdTe (MCT) is a very popular material system for IR detection and imaging, because it gives access to very high performances: high quantum efficiency (QE) together with low dark current. Partly due to its excellent performances, it is widely used for IR sensing from space. Luckily, it appears that this material system has the reputation of being a relatively radiation hard material, which is a real asset for space operation. The appearance of a credible alternative to MCT for space, namely III-V T2SLs or XBn InAsSb, raises the question of the comparative behavior of those different material systems, in terms of performance [1] [2] as well as radiation hardness. This rad-hard comparison between II-VI and III-V was first addressed by [3] using single diode devices mostly, focusing on first order figure of merit (QE, dark, lifetime…) confirming the robustness of II-VI over III-Vs. Other studies implying alternative substrates are not so conclusive [4]. Therefore, there is a real need about the understanding of radiation damage in IR detector systems, so that the actors of the space industry can make truly informed choices. In France, different actions are currently addressing this issue, for instance a study of radiation damages in MW-T2SL barrier structures, fabricated at IES-Montpellier Univ [5] or another study at III-V lab focusing InGaAs [6]. This paper reports on ongoing efforts at LETI, ADS and ISAE-SUPAERO about the fundamental understanding of radiation damage induced by gammas and protons on MCT n/p devices (diodes and FPAs) in the MW band, fabricated at LETI. The idea is to rise the fluence far above usual end-of-life doses (close to 10^{12}proton/cm² for instance) and extensively study the radiation induced damages, both in terms of QE/dark, but also in terms of noise and especially random telegraph noise (RTN). We will mainly focus here on the Displacement Damage Dose (DDD) in the MCT narrow gap semiconductor, (ie the electrical effect of permanent crystal defects induced by protons in the sensitive semiconductor). However, as protons might also induce ionizing effects, Total Ionizing Dose (TID) was also assessed on the same objects, using gamma irradiation in order to be able to differentiate DDD and TID.

* olivier.gravrand@cea.fr; phone +33 438 78 30 11

2. EXPERIMENTAL SETUPS

This study focuses on n/p VHg doped MCT diodes LPE grown in MWIR range, using LETI-Lynred legacy technology [7]. The irradiated samples were manufactured at CEA-LETI, including

- Variable size single diodes (from 10 to 120µm diameter), flip-chipped on Si fan-outs (therefore rear-side illuminated),
- P-type large size Metal/Insulator/Semiconductor (MIS) structures,
- Low doped P-type Van Der Paw hall effect samples,
- and 15µm pitch Focal Plane Arrays (FPA), 640x512 format, substrate removed, hybridized on a Direct Injection (DI) Read Out Integrated Circuit (ROIC) [8]

Those different samples were fabricated at LETI. Except Van der Paw samples which has a different doping level, the MCT devices are taken from the same MCT wafers, with a 5.2µm cut off wavelength at 78K. Si ROICs are CL274, from Lynred, Flip-chip hybridization, substrate thinning and packaging were performed at LETI.

Gamma irradiations were carried out at CEA-ARC Nucleart, using a C60 gamma source. The dose rated was 70krad(Si)/h to reach a maximum dose of 80krad(Si). Proton irradiations were performed at Université Catholique de Louvain (UCL) using a 55MeV proton beam. Typical targeted final dose was 8 10^{11} protons/cm² for a 130 krad(Si) equivalent TID.

Those irradiation and measurements were carried out in a variable temperature cryostat with f/8 FOV so that response variation was estimated using different BB temperature scenes (typically 20-30°C) at low detector temperature (typically 90K) and dark current degradation was assessed at higher temperature (up to 155K).

Diodes and MIS were cooled down at cryogenic temperature during irradiations. Pre-irradiation as well as post irradiation characterizations were carried out during the same thermal cycle, ie with no return to ambient temperature. Additionally, extra characterizations were also performed after a thermal cycle to room temperature (RT). In other words, the cryostat heated up to ambient temperature during the night after irradiation, then was cooled down again to perform extra characterizations.

3. IRRADIATION OF LOW COMPLEXITY SAMPLES

3.1 Assessment of dark current evolution on single diodes

Figure 1 shows IV performed on single diodes before and after (a) proton irradiation (8.15 10^{11} protons/cm²), and (b) gamma irradiation (80 krad(Si)), detector temperature during irradiation was 90K. Then diode temperature was set to 135K for characterization so that dark current dominates diode current. Therefore, the difference in current may not be related to QE fluctuation but dark current only.

As clearly shown on Figure 1a, proton irradiation strongly affects the IVs: the dark current increases for all reverse biases. After the thermal cycle to ambient temperature, an additional dark current contribution appears for biases between -0.5 and -1.5 V. Indeed, before thermal cycling, the IV is affected by irradiation but the general shape (diffusion plateau at low biases, below 1V, followed by tunnel current) remains. After thermal cycling, the transition between plateau and tunnel regime is very degraded and very dispersed from one diode to the other. Hence, defects induced by proton irradiation might not be all active at first and need some thermal energy to be fully activated/reorganized.

In contrast, gamma irradiation shown on Figure 1b did not change the measured dark current onto the whole bias range investigated even after the thermal cycle to ambient, independently of the state of polarization of the diode during the irradiation.

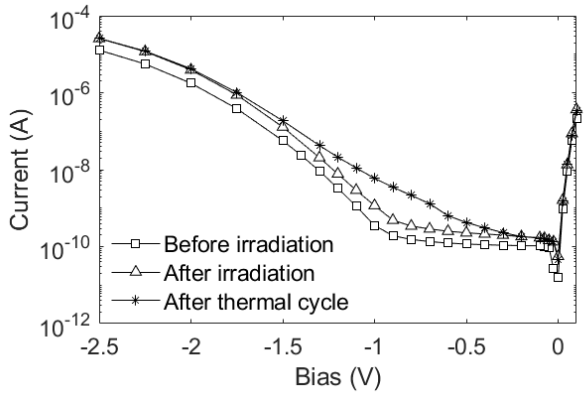

(a) Proton irrad.

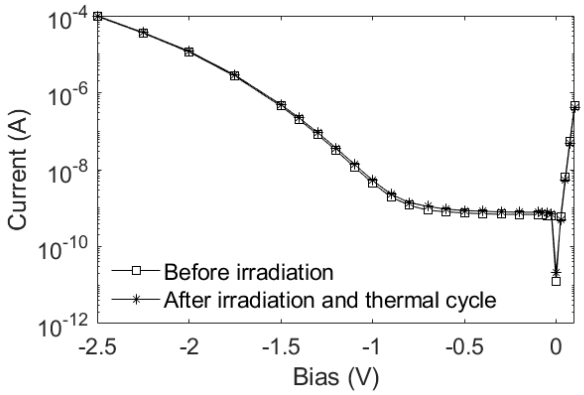

(b) Gamma irrad.

Figure 1: Example of single diode IV before, after irradiation and after RT thermal cycle (Temperature 135K)
(a) proton irradiation, 8.15 10^{11} protons/cm²
(b) proton irradiation, 80 krad(Si)

Going further into the analysis of this irradiation induced degradation of the dark current; Figure 2 shows the thermal evolution of a proton irradiated diode after thermal cycle, from 90K up to 155K. In this example, the plateau is limited to very low biases (100mV), and the diode switches to the irradiation induced leakage regime for higher but relatively low biases, in the 100mV range typically. Table 1 gives the extracted activation energies from Figure 2 for three different biases, and at three different steps of the irradiation campaign (before irradiation, just after the irradiation and after the RT thermal cycling). On the plateau, at -80mV, the extracted activation energy is close the 200meV, ie close to the band gap energy, suggesting a diffusion limited current. At -700mV, ie in the transition between plateau and tunnel, this activation energy decreases to a value closer to half the band gap after irradiation, and strongly decreases to much lower values after thermal cycling: the excess current appearing with RT thermal cycling appears then weakly depending on temperature. Finally, Table 1 gives extracted activation energies from -2V current, corresponding to the tunnel inverse regime. Low negative values are seen, characteristic of band-to-band tunnelling in HgCdTe photodiodes.

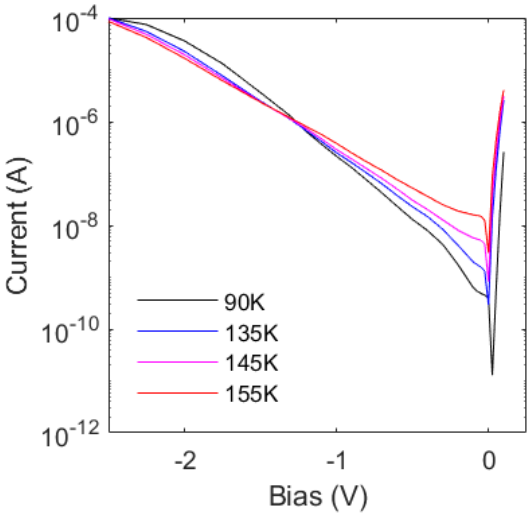

Figure 2:Evolution of a single diode IV with temperature, after proton irradiation 8.15 e11 protons/cm² and RT thermal cycle

Table 1. Activation energies extracted from Figure 2

Reverse bias	*-0.08 V*	*-0.7 V*	*-2 V*
Activation energy before irradiation (mev)	189	179	-65
Activation energy after irradiation (mev)	192	119	-38
Activation energy after thermal cycle (mev)	191	55	-27

These different considerations help us to determine the source of these different excess currents induced by the irradiation. Diffusion current tend to be very weakly affected by proton irradiation; whereas proton irradiation induced damages tend

to strongly increase tunnel current contribution and/or generation-recombination current in the depleted region of the photodiode.

3.1 Evolution of the proton damage on variable size single diodes

The evolution of dark current with diode geometry is also very instructive. Figure 3 gives an example of evolution of dark current with the n-type implantation area, at -500mV bias, 155K. It shows that the dark current degradation seems linear with the area. This effect is in fact seen for all biases, suggesting that the defects responsible for this dark current degradation (at intermediate bias, -500mV) are located in the depletion region.

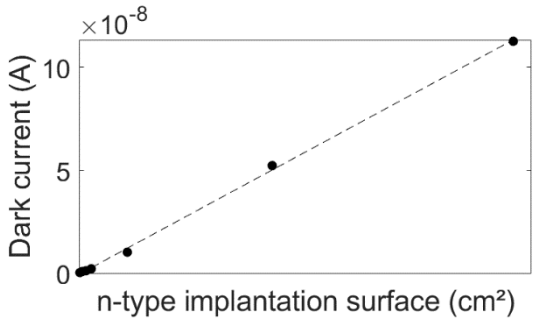

Figure 3: Irradiated diode dark current degradation extracted at -500mV bias, 155K, plotted against n-type implantation area

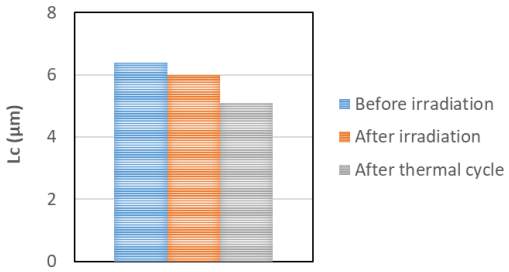

Figure 4: Extracted lateral collection at 90K from variable geometry single diodes biases at -80mV, before irradiation, after 8.15e11 protons/cm² irradiation, and after thermal cycle.

After irradiation, single diodes tend also to show a little loss in optical response (in the range of few percent only, but significant given our measurement setup). Such an effect was already observed in the literature [3]. This relative loss appears larger for smaller diode than for larger ones, suggesting a contraction in lateral collection. Indeed, those diodes are single planar diodes, ie not place within an array of pixel diodes. There sensitive areas are therefore limited by lateral diffusion of minority carriers. Fitting the photocurrent with diode geometries then allows for an estimation of this lateral collection, given in Figure 4. This lateral collection estimator first decreases a little with proton irradiation, then decreases again after the RT thermal cycle. The decrease in lateral collection length is probably related to the introduction of trap levels in the p-type material surrounding the diode, effectively decreasing the minority carrier lifetime. Such an effect has already been mentioned in the literature [9].

3.2 Van Der Paw and MIS samples, under proton or gamma irradiation

To go further, Van Der Paw samples [10] were also irradiated to assess possible doping changes in the absorbing narrow gap layer. In order to chase any change in VHg density, we chose a low doped P-type sample, in the 10^{-15} cm^{-3} range. The samples were irradiated at room temperature, and one of them was irradiated up to a very high dose, in the range of 3×10^{12} p/cm². Unfortunately, Hall Effect at room temperature as well as at 77K did not show any change, both in terms of charge density and mobility. Furthermore, photoluminescence decay (PLD) was performed on those samples à 77K, before and after proton irradiation, in order to assess any change in minority carrier lifetime. Yet, those measurements showed no noticeable change in the lifetime with irradiation.

Both measurement (Hall effect and PLD) thus suggest no clear creation/annihilation of VHg during irradiation. However, one limit of this approach lies however in the fact that samples were irradiated at room temperature, not at cryogenic temperature. Therefore, direct comparison between previous observed diode variation with irradiation (where diodes were cooled down to 90K during irradiation) and those estimated transport properties (where samples were kept at room temperature during irradiation) is not straightforward.

In order to probe the effect of irradiation onto the interface properties, we irradiated MIS structures, available on the same wafer than the diodes (so that the material and interfaces are comparable). Examples of typical MIS CVs are shown on Figure 5a for proton irradiation and Figure 5b for gamma irradiation. The interpretation of such curves is usually very

difficult because MIS CV is a very sensitive probe to various effects such as doping in the vicinity of the interface, but also fixed and mobile charges in the passivation, as well as the density of interface trap states.

First, gamma irradiation did not changed anything on MIS CV, whereas protons seemed to affect it: the first observation is that hysteresis are very similar, indicating that irradiation has no main effect onto the mobile charges in the passivation layer. Besides, post irradiation CVs exhibit a small decrease in the maximum capacitance, followed by a strong decrease after RT thermal cycle. This could indicate that close to the interface, the doping level tend to decrease with proton irradiation. This effect is then strongly enhanced with the thermal cycle, with an estimated decrease in doping of almost a factor of 2. Flat band voltages tend also to increase after thermal cycle, suggesting a p-type narrow gap semiconductor close to inversion underneath the passivation interface.

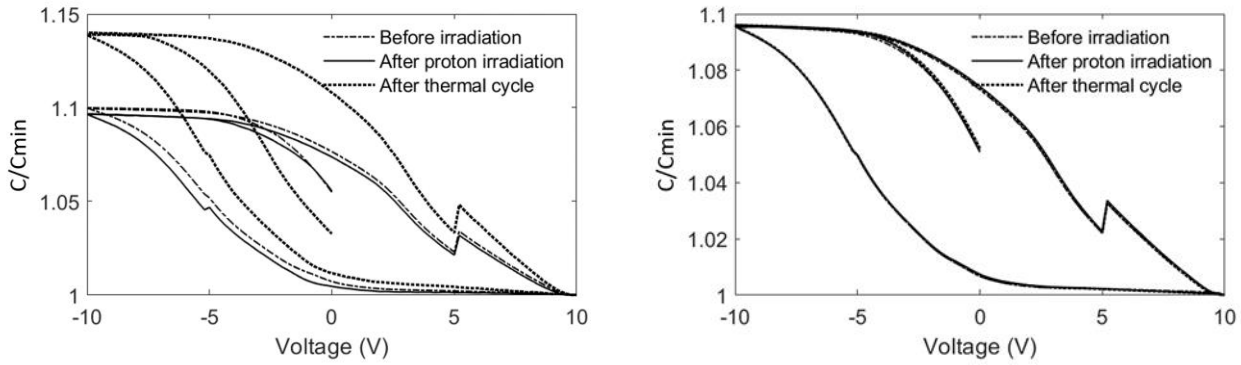

(a) Proton irrad. (b) Gamma irrad.

Figure 5: Example of MIS CVs before and after irradiation (Temperature 135K)
(a) proton irradiation, 8.15 10^{11} protons/cm²
(b) gamma irradiation, 80 krad(Si)

A preliminary conclusion would be that proton irradiation induced damage clearly affects the dark current, mostly for high biases. This suggest an increase in tunnel currents, probably assisted by radiation induced traps in the narrow gap depletion region. This degradation is even much worst after a thermal cycle to ambient temperature, suggesting a reorganization/activation of those defects with the associated thermal energy. At lower biases (usually used to operate such diodes), this dark current degradation is however not dramatic, probably hidden by the fact that the optical response of those single pixels is also slightly degrading with irradiation and thermal cycle. This response small variation might be related to a small decrease in carrier lifetime with a consequence on the lateral collection those single pixels and therefore on the sensitive area of the single diode.

4. IRRADIATION OF FOCAL PLANE ARRAYS

Previous considerations were based on single diodes, with no possible access to any statistical behavior. This section will focus on measurement carried out on higher complexity focal plane arrays, with access to close to 330 kpixels. The aim is now to investigate the statistics of the irradiation damage. Moreover, the use of a Si ROIC to drive those numerous pixels gives also easier access to noise properties of those diodes. This study array is divided into 16 variants with different diode flavors, mainly related to diode geometry, ie space charge region (SCR) width. Additional details on this device and the experiments done with it are given in [11] and [12]. Figure 6 left gives an example pre-irradiation current mapping, where those different diode flavors exhibit small differences in current, clearly distinguishable by different color shades. The corresponding current histogram (Figure 6 right) therefore exhibits different populations, but a low distribution tail: only few pixels have current in excess to 30pA. Note that the FPA is not in complete darkness: the given current mapping is mostly dominated by photonic current (f/8 ambient black body illumination). Note also that the bias used (300mV) is relatively high (close to the diffusion plateau-tunnel regime knee, see Figure 1) in order to easily track any change in tunneling current.

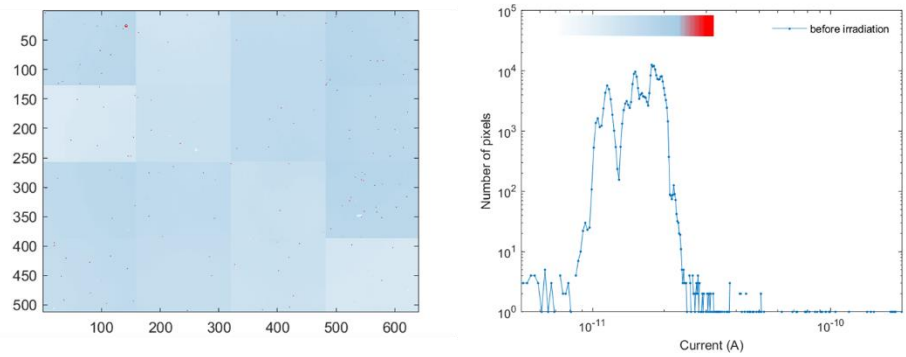

Figure 6: Pre-irrad current mapping and histogram of the FPA at 80K, inverse bias on the diodes is 150mV

4.1 Current statistics evolution with proton irradiation and annealing

This device was first proton irradiated in a liquid N2 cryostat, operating at 78K. Figure 7a shows corresponding current histograms at different dose steps of the irradiation sequence, namely 0.1, 1, 3 and 8 10^{11} protons/cm². During this irradiation sequence, the device was not biased. Clearly, a distribution tail towards high currents appears and grows with fluence after 10^{11} protons/cm²: hot pixels (ie pixels with a current larger than the photocurrent) appear with irradiation. Moreover, this distribution tail is even worst after thermal cycle to ambient. After this thermal cycle, the number of hot pixels is multiplied by almost a factor of 4. At this stage, about 2% of the pixel are detected as hot pixels. Those observations appear consistent with the dark current increase seen on single diode, except that only the dark current distribution is accessible with the FPA setup.

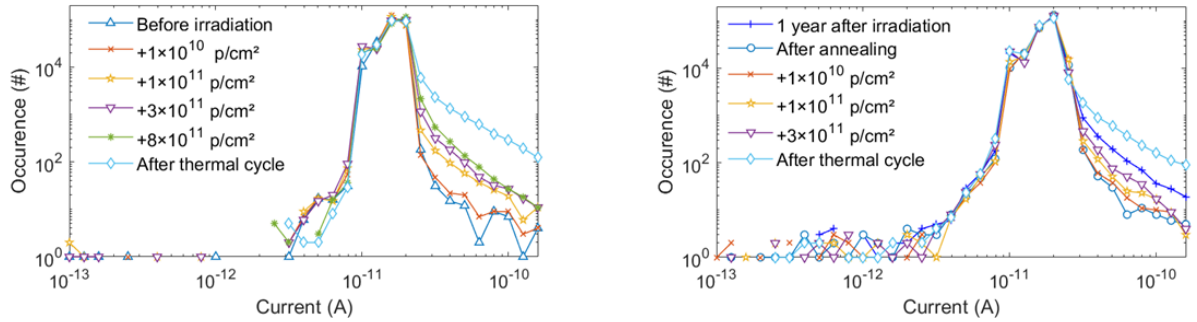

(a) 1st campaign, 78K, FPA unbiased (b) 2nd campaign, 90K biased

Figure 7: Measured current distributions on one full FPA, before proton irradiation, at different irradiation fluences and after a thermal cycle to ambient temperature, measurement bias 800mV
(a) first irradiation campaign, at 78K, FPA irradiated unbiased during irradiation
(b) second irradiation campaign, at 90K , FPA biased during irradiation

After a one-year rest, the device was characterized again at 90K, Figure 7b. It appears that the distribution tail decreased a bit, to the same level as before the RT thermal cycle, but remained strong. Then a warmer annealing was applied to the FPA, namely several hours above 80°C. After this annealing, the FPA almost fully recovered from the effect of the first irradiation, with a current distribution very similar to the pre-irradiation one. So, this FPA was used for a second irradiation campaign. A different cryostat was used, allowing variable operating temperature for further studies. This time, the FPA was cooled at 90K and was biased during all proton irradiation steps, as opposed to previous campaign where the FPA was open circuited at 78K.

Figure 7(b) shows the resulting current histograms. Despite experimental differences, the results are very similar for the three investigated fluences 0.1, 1 and 3 10^{11} p/cm²: the distribution tail rises with irradiation with a very comparable rate (see also Figure 8). This time however, after irradiation, different thermal cycles have been investigated. A first rise from 90K to 135K then back to 90K showed no noticeable difference in the current distribution. A second rise to 155K did not show any important change as well. In the end, the final RT thermal cycle resulted once again in a strong increase in hot pixel count, as summarized in Figure 8.

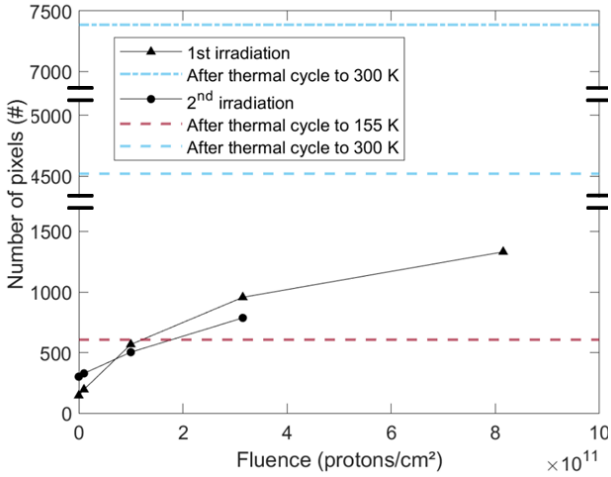

Figure 8: Summary of the evolution of the number of hot pixels with fluence and thermal cycle

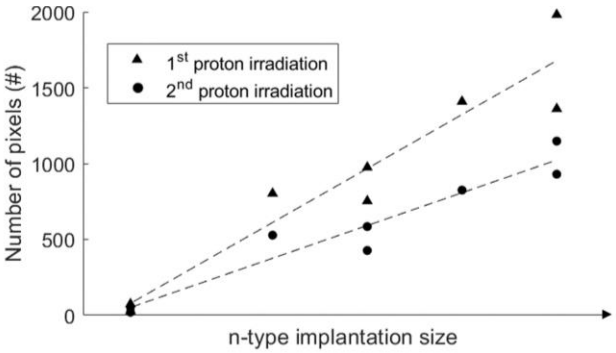

Figure 9. Evolution of the number of hot pixels with junction size, after thermal cycle
1st proton irradiation $8 \times 10^{11} p/cm^2$
2nd proton irradiation $3 \times 10^{11} p/cm^2$

As mentioned previously, this FPA contains different diode geometries, and the current distribution tails appear different in each of those diode variants. Plotting the hot pixel density against diode implantation size reveals a clear correlation between the numbers of irradiation induced hot pixels and the width of the diodes. Both irradiation campaign exhibit the same behaviour, see Figure 9). Indeed, larger diodes exhibit larger distribution tails. Given the small variation allowed in a 15µm pitch, it is however difficult to really assess if this increase is proportional to the diode area or proportional to the junction width (ie the diode perimeter). Still, measurement on single diode showed that the dark current increase tend to scale with the area rather than the width.

As mentioned previously, dealing with hot pixels means dealing only with the tail of the dark current distribution. Given the geometry of the cryostat used (f/8) and the DI input stage of the ROIC, the dark current is not accessible. However, at 135K, the dark current overcomes the photocurrent and the full dark current distribution is therefore accessible, large enough to be measured by the ROIC. At this temperature, the main distribution measured for 3 10^{11} p/cm² then shifts with irradiation from roughly 23pA to 30pA, representing a 30% increase in dark current.

After proton irradiation, we also observed a small loss in pixel response, smaller than 4% at 1 10^{11}p/cm², scattered between 8 and 1% at higher fluence, 1 10^{11}p/cm². This loss in response is lower for larger diodes than for smaller ones, probably related to the collection length change, consistent with assessment made on single diodes.

4.2 RTS statistics evolution

Another well-known radiation induced behavior is the emergence of random telegraph signal (RTS), also called burst or flicker noise. Such an effect has been observed on different material systems [13] such as Silicon transistors or diodes [14], in particular in Si solid-state imagers [15] or even narrower semiconductor materials such as InGaAs [16] and InSb [17]. RTS has also been observed and studied in MCT [18][19][20]. In this work, we performed long data cubes (5000 successive image acquisitions at a 4Hz frame rates during 20min) in order to study low frequency noise behavior of damaged pixels. RTS pixels were then detected using a well know and public algorithm given in [21], based on an edge detection approach.

Figure 10 shows an example of the temporal trace of a damaged pixel, throughout the different steps of the first proton irradiation at 78K. This pixel is in its normal state before irradiation (low dark current, shot-noise limited). After a 2$10^{11}$ p/cm² fluence, this pixel exhibits two distinct states, detected by the algorithm. At a larger fluence 8 10^{11}p/cm², this

given pixel appears more agitated and the algorithm detects clearly more than two levels, with higher overall amplitude transitions. Hence, RTS analysis might be very complex, given the large number of parameters involved (transition amplitude, frequency, and characteristic time in one state…). For the sake of simplicity, we will focus our analysis on few parameters: the total number of RTS pixels detected by the algorithm, and for each detected pixel, the number of RTS transitions in the measurement (ie the blinking rate), the number of RTS levels and the maximum transition amplitude.

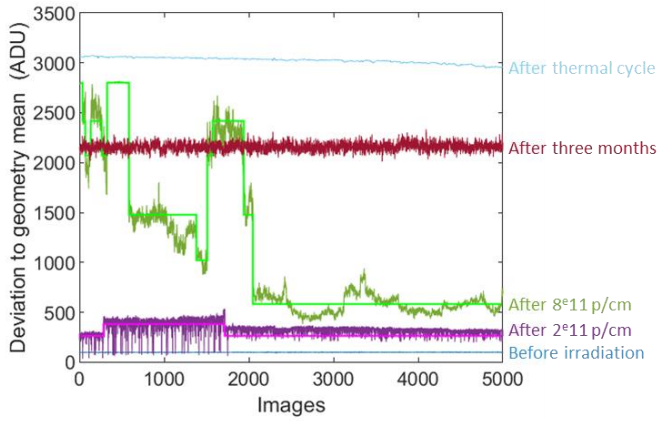

Figure 10: Example of temporal RTS trace of a given pixel affected by proton induced damage, at the different irradiation stages

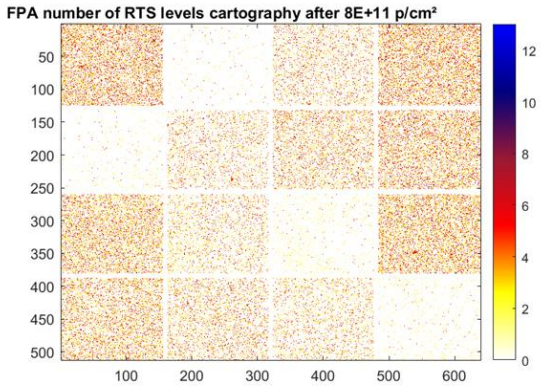

Figure 11: RTS level number mapping, after 8 10^{11} p/cm², Different diode flavours gives different RTS pixel densities.

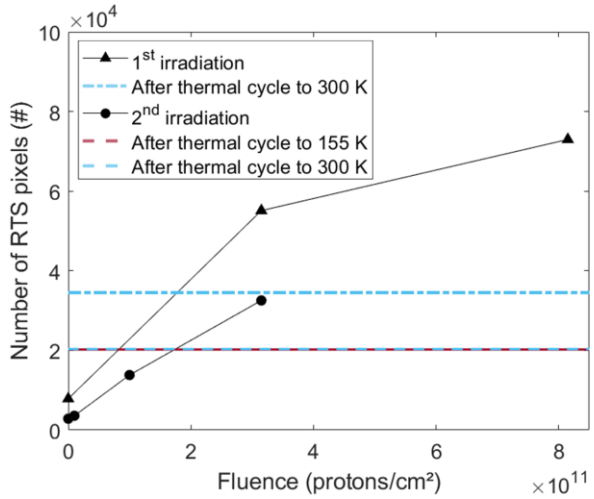

Figure 12:Number of RTS detected pixels with fluence during the two irradiation campaigns and effect of thermal cycling and annealing

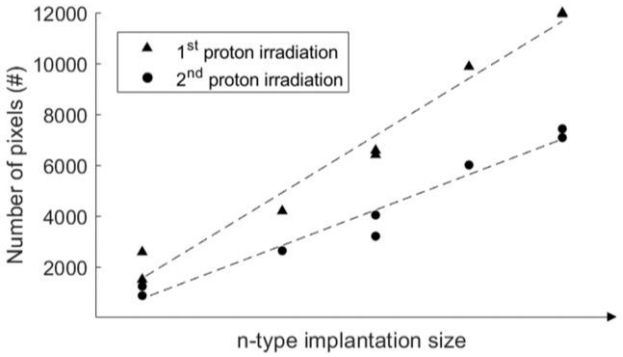

Figure 13: Evolution of the number of detected pixel with diode width, after 3 10^{11} p/cm²

As expected, the total number of RTS pixels increases with fluence as shown in Figure 12. However, as opposed to what was observed with dark current, the number of RTS pixel clearly decreases with thermal cycling, but do not reach its initial state. After the warmer 80°C annealing however, RTS activity goes back to its level before irradiation.

During the second irradiation campaign, the RTS pixel total number increases at a slightly lower rate than before, but experimental conditions were slightly different (detector temperature was 90K instead of 78K, FPA was biased during irradiation, optical flux might be a little different…). Nevertheless, the trend remains the same: higher fluence give more RTS pixels. A last interesting point from Figure 12 is that a 155K thermal cycle gives the same effect as the RT thermal cycle, soothing the global RTS behavior, which is different from the observations made on dark currents.

It is worth noticing as well that the density of RTS pixels depends also on the pixel design. Figure 11 shows for instance the spatial mapping of the detected RTS level number distribution after 8 10^{11} p/cm², and the different diode flavors are clearly visible with different densities. The total number of detected RTS pixels is clearly depending on pixel size: the larger the pixel, the more RTS, as shown for instance on Figure 13. However, with the dimensions available in a 15µm pitch, it is once again not possible to assess here if RTS density depends on diode surface or diode perimeter.

Going further, Figure 14 gathers those RTS distribution (number of levels on the left plot and maximum amplitude on the right plot) at the different steps of the proton irradiations: First campaign at 78K, before irradiation, at 3 and 8 10^{11} p/cm², after RT thermal cycling, and then after the 80°C annealing. The plots also show distributions obtained during the second irradiation campaign at 90K, for 0.1, 1 and 3 10^{11} p/cm², and after the final RT thermal cycle.

With the increase of the fluence, not only the number of pixels increases, but also these pixels seem to be more disturbed: the distribution goes up to larger number of RTS levels. One the other hand, the max amplitude distribution pleads for the same assessment: with higher fluences comes larger amplitudes. The RTS pixels are therefore more agitated increasing the fluence. Despite the slightly different experimental conditions, the two distributions (number of RTS levels and max amplitudes) appear very repeatable for both irradiation campaigns. This clearly demonstrates the ability of a simple 80°C annealing to delete the deleterious effects of previous proton irradiation.

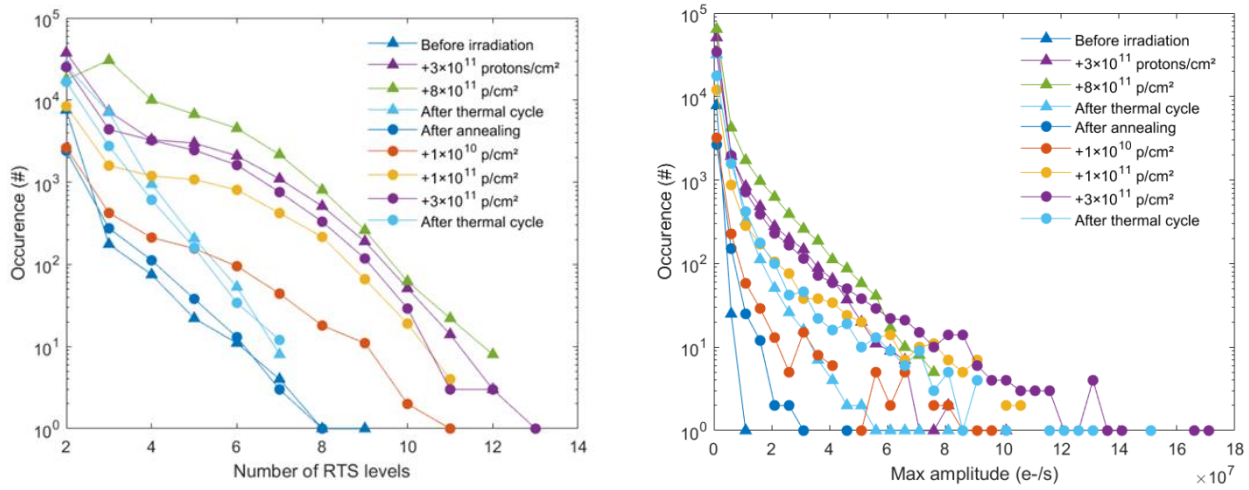

(a) (b)

Figure 14 Evolution of the RTS statsitics with fluence and thermal cycling.
(a) distribution of the number of RTS levels
(b) distribution of the max amplitudes of RTS pixels
Triangular marked curves are for the first irradiation with no applied bias and a device operated at 78 K. Circle marked curves are for the second biased irradiation with temperature device of 90 K.

Figure 14b calls also for another comment. Previous studies of radiation induced RTS for Si or InSb reported an exponential amplitude distribution, both before and after irradiation [15] [17]. Here, in Figure 14b, distributions appear not perfectly exponential. Indeed, it features an additional bend toward higher amplitudes such that the distribution appear more log-log than normal-log as expected (it aligns along a straight line in log-log scale rather than in semi-log scale). This suggests a different behavior than classically observed in silicon. One explanation could be related to electrical field enhancement effect. Therefore, the effect of junction electric field in the diode was also investigated. We will discuss here only some few elements. The interested reader can consult [11] and [12] for further details.

In short, at 90K, the number of RTS pixels is highly depending on the bias applied to the diode, ie on the electric field in the space charge region. Indeed, the number of detected pixels was multiplied by close to 7 just increasing the bias from - 300mV (V_{fpa}=0.8V) to -900mV (V_{fpa}=1.4V). Focusing on the RTS pixels identified at low bias, Figure 15 shows the evolution of the RTS properties of this given pixel population. Both the number of RTS transitions and the number of RTS levels exhibit identical distributions at both biases. Only the maximal amplitudes increase with this 600mV bias increase.

However, the amplitude distributions do not have the same shape. From a close to exponential shape at low bias (ie a strong population with small amplitudes and a much smaller population with a larger amplitudes), we end up with a distribution exhibiting an intermediate plateau and even a small decrease of the population for low RTS amplitudes. This may be understandable in the sense that at low bias, very low amplitude RTS pixels tend to be hidden by the noise of the measurement (either from the photocurrent or from the read out noise). Those pixels are therefore not well identified and are not part of the distribution studied at higher bias. This might explain the lack of population seen on small amplitudes. This suggests that the electric field only modifies the blinking amplitude, but not the blinking frequency or the number of levels: the responsible defect is likely in the depletion volume, and should be active in the same way, but with higher current states. Of course, depletion volume is different in the two bias configurations and larger biases might gather more active defects (assuming a uniform creation of proton induced defects in in the narrow gap layer). Those additional defects investigated by the depletion extension are in fact not taken into account in the studied statistic of Figure 15.

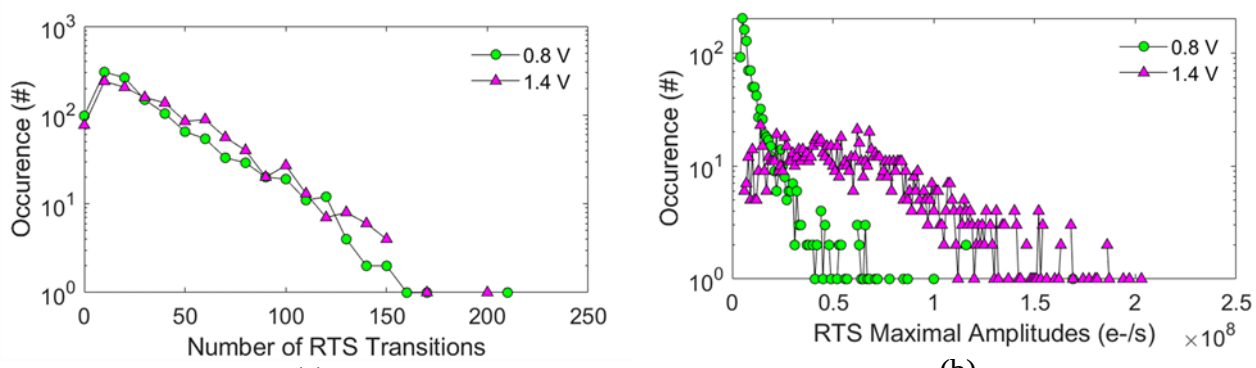

(a) (b)

Figure 15: Effect of the FPA operating bias Vpol (0.8V, 1.4V) on a selection of 2400 RTS pixels identified at 0.8V, 90K
(a) distribution of the number of RTS transitions
(b) distribution of the max amplitudes of RTS pixels

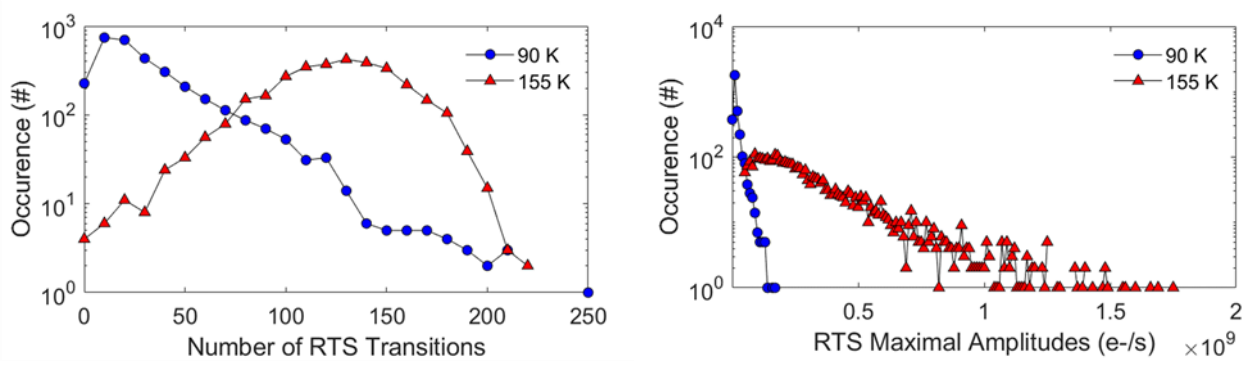

(a) (b)

Figure 16: Effect of temperature (90K and 155K) on a selection of 3200 pixel identified as RTS at 90K
(a) distribution of the number of RTS transitions
(b) distribution of the max amplitudes of RTS pixels

Last but not the least, proton induced RTS amplitudes appear to be thermally activated, with an activation energy close to mid-gap, suggesting an origin in the depletion region of the photodiode, consistent with the correlation between number of RTS pixels and diode size (Figure 13). Investigating deeper the statistics of those blinking pixels is also interesting. To that end, Figure 16 presents statistic characteristics of a selection of 3200 pixels identified as RTS at 90K. The figure shows the distribution at 90K, and how it changes going up to 155K. It shows that the statistics changes clearly between 90K and 155K. The blinking is faster, and going from 90K to 155K, the dark highly increases with an activation energy close to the gap (diffusion limit) whereas the RTS amplitudes strongly increases, but with a smaller activation energy, related to the

mid-gap as previously mentioned. Those results are very similar to pre-irrad RTS pixels thermal properties [19] and argue once more toward the depletion volume as source of RTS.

4.3 Effect of gamma irradiation on FPA operation

Another FPA was used for gamma irradiation, in order to specifically investigate TID rather than DDD, ie charge induced effects rather than crystal damage. The FPA was cooled down to 90K during irradiation and characterized in the same cooling cycle. A first irradiation up to 80krad(Si) with the FPA unbiased showed no change at all in the distribution, even after a RT thermal cycle. The same FPA was then irradiate biased, with an additional 30krad(Si). Short after irradiation, the current histogram did not change much. However this time, the effect of the RT thermal cycle was very noticeable: an important distribution tail appeared for low current: the gamma irradiation under bias induced a lot of cold pixels after thermal cycle, see Figure 17. As opposed to proton damages, this time, the gamma induced distribution tails do not depend on pixel geometry, as shown on Figure 18, thus suggesting an effect related to the Si ROIC rather than the sensitive layer. Moreover, reset voltage measurement showed a significant shift (18%), supporting also Si as a source of this degradation under gamma irradiation.

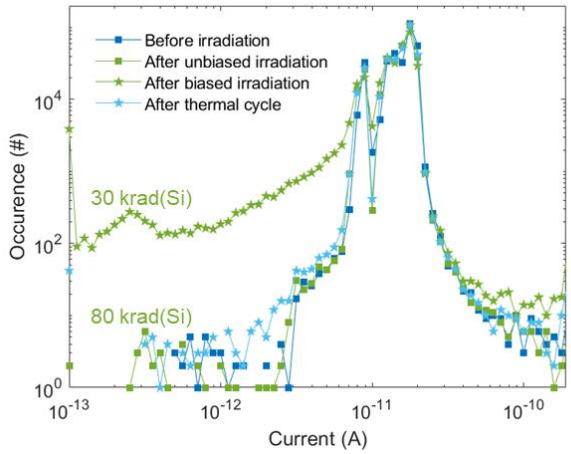

Figure 17: Effect of gamma irradiation on FPA current distribution.
(FPA @ 90K during irradiation and characterization).

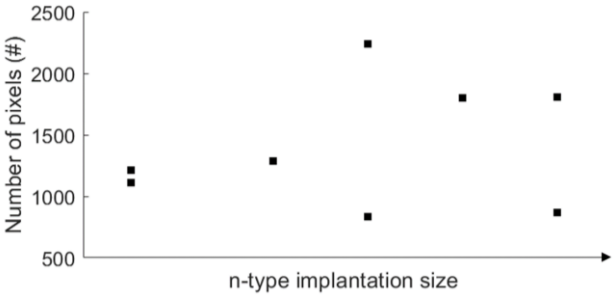

Figure 18: Evolution of the number of cold pixels with diode size after 30krad(Si) gamma irradiation biased followed by thermal cycle

As previously in the proton irradiation campaigns, RTS measurements were also performed during those gamma irradiation campaigns and the conclusion are very similar as for current distribution. There was no increase of RTS statistic within the first campaign at 78K, with FPA unbiased during irradiation. However, after the second campaign, were the FPA was biased at 90K during irradiation, 8.5% of the total pixel population were detected as RTS. This number went down to 0.8% after RT thermal cycle. Again, the pixel design has no influence on RTS occurrence and statistics. Consistently with the current distribution variation, this points again toward the ROIC as a source for degradation with TID when the device is biased during irradiation.

5. DISCUSSION AND CONCLUSION

In this work, n/p MW MCT photodiodes have been irradiated with gammas for TID assessment, as well as protons for DDD. High fluences were considered, in order to comfortably study the radiation-induced damage of diodes and FPAs. Gamma did not seem to affect single diodes, even when biased during irradiation. However, the Si ROIC appeared strongly affected by TID when biased: cold pixels appeared, and the density of those cold pixels is not related to diode variants.

Proton irradiation however affected single diode dark current. The IV curves were lightly degraded immediately after irradiation, but significantly worsened and distorted after a room temperature thermal cycle.

Diffusion dark current at low biases increased weakly, even at very high doses. In the same time, the diode response appeared to be lightly degraded as well, due to a contraction of the lateral collection length. Both observations are consistent with a degradation of the minority carrier lifetime in the p-type diffusion narrow gap material, despite the fact that we have not been able to prove it with doping or PLD lifetime measurements. On the contrary, CVs performed on MIS structures indicate a significant lowering of the doping beneath the passivated front interface. Such a close to inversion interface could also be source of side leakages between neighboring diodes in an array. As this effect has not been clearly seen with gamma irradiation, this effect is a priori linked to a change in the properties of the small gap interface (doping, DIT,...) rather than a charge effect in the passivation.

On the other hand, for higher biases the dark current showed a strong increase with proton irradiation, particularly after RT thermal cycle. This excess dark current scales very well with the junction area, pointing a depletion related source. For intermediate bias, the activation energy associated to this dark current appears to be close to half the band-gap, consistently with a depletion GR excess dark current. For higher biases, this activation energy turns negative, indicating tunnel contributions (the gap increases with increasing temperature in MCT).

Irradiated FPAs gave us a picture similar in terms of dark current. Because of the limitation of the input stage for very low current, dark current was not directly accessible. The main dark current distribution was hidden below photonic current, so that only dark current distribution tail toward high currents was available in the measurement. Indeed, the behavior of this tail appeared very consistent with the observations performed on single diode: this tail increases with fluence, bias and with junction geometry. Moreover, gets much worst with RT thermal cycle.

However, the proton irradiation not only induced dark current excess. It also generated low frequency noise in some pixels. This was manifested by RTS with variable numbers of levels, various jump frequencies, and various jump amplitudes. The detailed study of those RTS revealed some similitudes with the proton-induced effect on dark current: amplitudes and frequencies were thermally activated with temperature with an activation energy close to mid gap, and was enhanced by electric field. Also, more pixels were affected with larger pixel geometries, and larger fluences.

Until now the picture seems relatively clear: all those clues points toward the generation of uniformly distributed proton-induced defects. When those defects are located into the p-type diffusion layer, some of them might be electrically active, as local generation-recombination centers, thus degrading the diffusion dark current. When immerged into the depletion region of the photodiode however, the electrical activity might be stronger due to the electrical field, thus generating larger excess dark currents through assisted tunneling mechanisms, or more simply through GR current for lower fields.

However the parallel between proton-induced dark current and RTS pixels stops there. Indeed, the electrical activity of those proton-induced defect seems unstable: a simple room temperature thermal cycle appeared enough to strongly modify this activity giving higher excess dark currents, as if these defects were able to reconfigured with this low temperature annealing and ended up in a more electrically active state. Nevertheless, this effect was not observed on RTS pixels. On the contrary, the same RT thermal cycle seemed to decrease the RTS activity, with lower amplitudes, lower frequencies, and lower number of levels. As a logical consequence, a lower number of pixels was detected, given the noise floor of the measurement. To take this discussion a step further, it is then possible to mention raising the temperature from 90K to 155K had an annealing effect on the RTS, whereas it had no effect on dark current.

Finally, it also worth noticing that a simple annealing to 80°C appeared sufficient to cure all the proton-induced damages, both in terms of dark current and RTS, and the FPA was back into its original shape. Therefore, reasonably higher thermal energies appears sufficient to repair all the proton induced damages in the narrow gap MCT layer, and in the end, the weakest link in the device was finally the Si ROIC, which ended up non-operational for very large fluences, probably more damaged by TID than DDD.

6. ACKNOWLEDGMENTS

The authors would like to thank CNES for its support for beam time, as well as ArtNucleart for its gamma facility and UCL for proton facility.

REFERENCES

[1] P. Martyniuk and A. Rogalski, (2014), "*Performance comparison of barrier detectors and HgCdTe photodiodes*" SPIE, 907014, https://doi.org/10.1117/12.2057502

[2] M. Kinch, (2015), "The Future of Infrared; III–Vs or HgCdTe?," J. Electron. Mater., vol. 44, no. 9, pp. 2969–2976, https://doi.org/10.1007/s11664-015-3717-5

[3] Jenkins, G. D., Morath, C. P., & Cowan, V. M. (2017). "*Empirical Study of the Disparity in Radiation Tolerance of the Minority-Carrier Lifetime Between II–VI and III–V MWIR Detector Technologies for Space Applications*. Journal of Electronic Materials, 46(9), 5405–5410. https://doi.org/10.1007/s11664-017-5628-0

[4] E. H. Steenbergen, C. P. Morath, D. Maestas, G. D. Jenkins, and J. Logan, (2019), "*Comparing II-VI and III-V infrared detectors for space applications*" , SPIE 110021B, https://doi.org/10.1117/12.2519250

[5] C. Bataillon *et al.*, (2023), "*Dark current behaviour of type-II superlattice longwave infrared photodetectors under proton irradiation*," *Opto-Electronics Rev.*, vol. 31, 2023, https://doi.org/10.24425/opelre.2023.144552

[6] M. Benfante et al.(2023), "*Electric Field Enhanced Generation Current in Proton Irradiated InGaAs Photodiodes*," IEEE Trans. Nucl. Sci., vol. 70, no. 4, pp. 523–531, https://doi.org/10.1109/TNS.2023.3244416

[7] G.L. Destefanis (1991), "HgCdTe infrared diode arrays", Semicond. Sci. Technol. 6, C88, https://doi.org/10.1088/0268-1242/6/12C/017

[8] F. Guellec *et al.*, "*ROIC development at CEA for SWIR detectors: pixel circuit architecture and trade-offs*" in *International Conference on Space Optics — ICSO 2014*, Nov. 2017, p. 152, https://doi.org/10.1117/12.2304212

[9] J. E. Hubbs et al. (2007), "*Lateral Diffusion Length Changes in HgCdTe Detectors in a Proton Environment* ", IEEE Trans. Nucl. Sci., vol. 54, no 6, Art. no 6, https://doi.org/10.1109/TNS.2007.910329

[10] L.J. van der Pauw, (1958), "*A Method of Measuring the Resistivity and Hall Coefficient on Lamellae of Arbitrary Shape*",Philips Technical Review. 20: 220–224

[11] Dinand, S., Gravrand, O., De Borniol, E., Baier, N., Rizzolo, S., Saint-Pe, O., Virmontois, C., & Goiffon, V. (2023). "*Design, Annealing and Electric Field Effects on Proton and Gamma Irradiated MWIR HgCdTe Focal Plane Arrays*". IEEE Transactions on Nuclear Science, 70(4), 1–1. https://doi.org/10.1109/tns.2023.3256562

[12] S. Dinand, V. Goiffon, D. Lambert, S. Rizzolo, N.Baier, E. DeBorniol, O. Saint-Pé, C. Durnez and O. Gravrand, "*Proton Radiation Induced Random Telegraph Signal in HgCdTe Photodiode Array*", to be published in IEEE Transaction on Nuclear Science, reports from RADEC 2022 in Venise, Italy.

[13] Srour, J. R., & Palko, J. W. (2013). "*Displacement damage effects in irradiated semiconductor devices*". IEEE Transactions on Nuclear Science, 60(3), 1740–1766. https://doi.org/10.1109/TNS.2013.2261316

[14] Dewitte, H., Member, S., Goiffon, V., Member, S., Roch, A. Le, Rizzolo, S., Virmontois, C., Marcandella, C., & Paillet, P. (2022). "*Radiation-Induced Junction-Leakage*". IEEE Trans. Nucl. Sci. 69(3), 290–298. https://doi.org/10.1109/TNS.2021.3119456

[15] Virmontois, C., Goiffon, V., Robbins, M. S., Tauziede, L., Geoffray, H., Raine, M., Girard, S., Gilard, O., Magnan, P., & Bardoux, A. (2013). "*Dark current random telegraph signals in solid-state image sensors*". IEEE Transactions on Nuclear Science, 60(6), 4323–4331. https://doi.org/10.1109/TNS.2013.2290236

[16] Barde, S., Ecoffet, R., Costeraste, J., Meygret, A., & Hugon, X. (2000). "*Displacement damage effects in InGaAs detectors: Experimental results and semi-empirical model prediction*". IEEE Transactions on Nuclear Science, 47(6 III), 2466–2472. https://doi.org/10.1109/23.903794

[17] Durnez, C., Goiffon, V., Virmontois, C., Magnan, P., & Rubaldo, L. (2020). "*Comparison of Dark Current Random Telegraph Signals in Silicon and InSb-Based Photodetector Pixel Arrays*". IEEE Transactions on Electron Devices, 67(11), 4940–4946. https://doi.org/10.1109/TED.2020.3022336

[18] Perez, J., Myara, M., Alabedra, R., Orsal, B., Leyris, C., Tourrenc, J., & Signoret, P. (2005). "*Low-Frequency Noise Measurements as an Investigation Tool of Pixel Flickering in Cooled Hg 0 : 7 Cd 0 : 3 Te Focal Plane Arrays*". IEEE Transaction on Electron Devices, 52(5), 928–933. https://doi.org/10.1109/TED.2005.846328

[19] Brunner, A., Rubaldo, L., Destefanis, V., Chabuel, F., Kerlain, A., Bauza, D., & Baier, N. (2014). "*Improvement of RTS Noise in HgCdTe MWIR Detectors*". Journal of Electronic Materials, 43(8), 3060–3064. https://doi.org/10.1007/s11664-014-3217-z

[20] Guénin, M., Derelle, S., Caes, M., Rubaldo, L., & Ribet-Mohamed, I. (2020). "*RTS Noise Detection and Voltage Effect on RTS in HgCdTe Focal-Plane Arrays*". Journal of Electronic Materials, 49(11), 6963–6970. https://doi.org/10.1007/s11664-020-08271-y

[21] V. Goiffon, P. Magnan, O. Saint-Pé, F. Bernard, and G. Rolland, "*Multi level RTS in proton irradiated CMOS image sensors manufactured in a deep submicron technology*", IEEE Trans. Nucl. Sci., vol. 56, no. 4, pp. 2132–2141, 2009. https://doi.org/10.1109/RADECS.2008.5782739